First determination of the Planck constant using the LNE watt balance

First determination of the Planck constant using the LNE watt balance

M Thomas[1], P Espel[1], D Ziane[1], P Pinot[2], P Juncar[2], F Pereira Dos Santos[3], S Merlet[3], F Piquemal[1] and G Genevè**s[1]**

[1] Laboratoire National de Métrologie et d'Essais (LNE), 78197 Trappes, France
[2] Conservatoire National des Arts et Métiers (CNAM), 93210 La Plaine St-Denis, France
[3] LNE-SYRTE, Observatoire de Paris, LNE, CNRS, UPMC, 75014 Paris, France

E-mail: matthieu.thomas@lne.fr

CrossMark

Abstract

After separate developments of the different elements with continuous characterizations and improvements, the LNE watt balance has been assembled. This paper describes the system in detail and gives its first measurements of the Planck's constant h. The value determined in air is $h = 6.626\,068\,8(20) \times 10^{-34}$ Js which differs in relative terms by -0.05×10^{-7} from the h_{90} value and by -1.1×10^{-7} from that of the 2010 CODATA adjustment of h. The relative standard uncertainty associated is 3.1×10^{-7}.

(Some figures may appear in colour only in the online journal)

1. Introduction

The kilogram is the last unit of the *Système International* of units (SI) still based on an artifact. It is defined by the mass of the International Prototype of the Kilogram (IPK) made from platinum-iridium alloy (Pt90%Ir10%) and stored at the BIPM in Sèvres [1, 2]. It was machined in 1878 as a number of other prototypes designated as official copies a few years later. Four of them are stored in the same conditions as the IPK. Thirteen others are the national prototypes used by the signatory countries of the *Convention du mètre*.

Since the 1880s, only three comparisons have been organized to survey the evolution of the mass of the official copies and national prototypes relative to IPK. The results display a relative drift of about 3×10^{-8} over the course of a century [3] which makes the current definition of the kilogram unsatisfactory. This situation is no longer acceptable in a time of ever-increasing measurement precision and for this reason, there is a strong desire among international laboratories to move to a new, more robust definition of the unit of mass [4–7]. For the past few years, significant efforts have been made to link the unit of mass to a fundamental constant of physics with high accuracy. National metrology institutes have essentially developed two experiments—a silicon sphere [8] and

watt balances [9–16]—to link the unit of mass respectively to the Avogadro and Planck constants. In 2001, the Laboratoire national de métrologie et d'essais (LNE) decided to develop a watt balance experiment in order to contribute to the international effort to redefine the kilogram. Twelve years later, after separate developments of the different elements with continuous characterizations and improvements, the entire system has been assembled.

The paper presents an overall description of the LNE watt balance, gives a first measurement of the Planck constant and analyses the main contributions to the uncertainty budget.

2. Principle of the watt balance

The watt balance principle proposed by Kibble in 1976 [17] consists in the comparison between virtual electromagnetic and mechanical powers measured during two steps (called static and dynamic phases) by means of a beam balance.

In the static phase (or force mode), the weight $m \cdot \vec{g}$ of a standard mass m subject to a gravitational acceleration $\vec{g}$ is balanced by the Laplace force $\vec{F}$ exerted on a coil of length l in which there flows a current I when the coil is immersed in a magnetic induction field $\vec{B}$. For perfect alignment of

the system (horizontal magnetic field, horizontal coil and vertical Laplace force), this equilibrium is described by the relation:

$$mg = (B \cdot l)_{\text{stat}} \cdot I \qquad (1)$$

where I may be measured by the voltage drop U' it produces at the terminals of a known resistance R.

In the dynamic phase (or velocity mode), the coil is moved at a vertical velocity $\vec{v_z}$ in the same magnetic induction field $\vec{B}$. Again for perfect alignment of the system, Lenz's law of induction leads to a voltage drop at the coil terminals given by:

$$U = (B \cdot l)_{\text{dyn}} \cdot v_z \qquad (2)$$

If the magnetic flux in both phases is the same (i.e. the same coil in the same magnetic induction), the combination of relations (1) and (2) can be re-expressed as the equality of virtual mechanical and electrical powers in SI units leading to:

$$(B \cdot l)_{\text{dyn}} = (B \cdot l)_{\text{stat}} \qquad (3)$$

In practice the voltages are linked to a Josephson effect voltage standard (via the Josephson constant K_J) and the resistance is linked to the quantum Hall effect resistance standard (via the Von Klitzing constant R_K). In this way, the mass m can be expressed in terms of the Planck's constant h, provided it is accepted that the product $K_J^2 \cdot R_K$ is equal to $4/h$ [18].

Since the Josephson effect and quantum Hall effect are used with the values conventionally defined in 1990, respectively $K_{J\text{-}90}$ and $R_{K\text{-}90}$, it follows that:

$$h = \frac{4}{K_{J\text{-}90}^2 \cdot R_{K\text{-}90}} \cdot \frac{mg}{\frac{U'_{90}}{R_{90}}} \cdot \frac{1}{\frac{U_{90}}{v_z}} \qquad (4)$$

Following the formalism [18], one can then write:

$$\frac{h}{h_{90}} - 1 = \frac{(B \cdot l)_{\text{stat}}}{(B \cdot l)_{\text{dyn}}} - 1 \qquad (5)$$

The relative difference between the value of the Planck's constant h in the SI and its value h_{90} expressed in terms of $R_{K\text{-}90}$ and $K_{J\text{-}90}$ is equal to the relative difference between the measured values of the product $(B \cdot l)$ in the static and dynamic phases.

3. LNE watt balance description

One of the characteristics of the LNE watt balance is that, during the dynamic phase, the force comparator (balance beam and its suspension) is moved as a single element by means of a translation stage actuated by a stepper motor, in order to avoid one's using the balance beam as the element generating the movement. Figures 1 and 2 show respectively a picture of the LNE watt balance and a schematic of the core of the system.

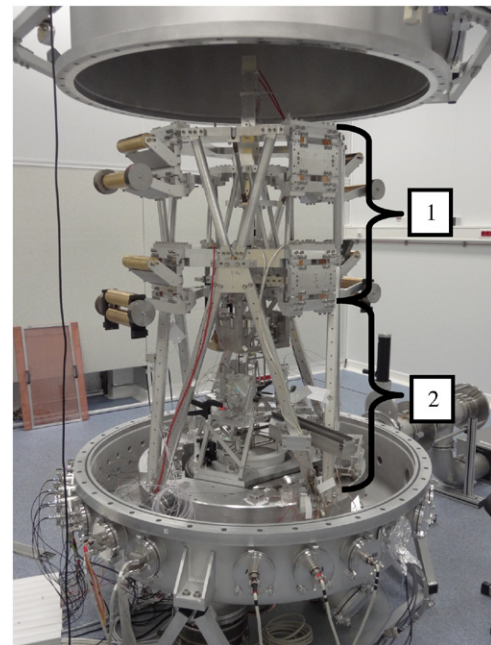The following subsections describe the experimental set-up that was used to obtain the first results of measurements h.

Figure 1. Picture of the LNE watt balance: translation stage (1) and force comparator with the coil and masses suspensions (2) (see figure 2 for more details).
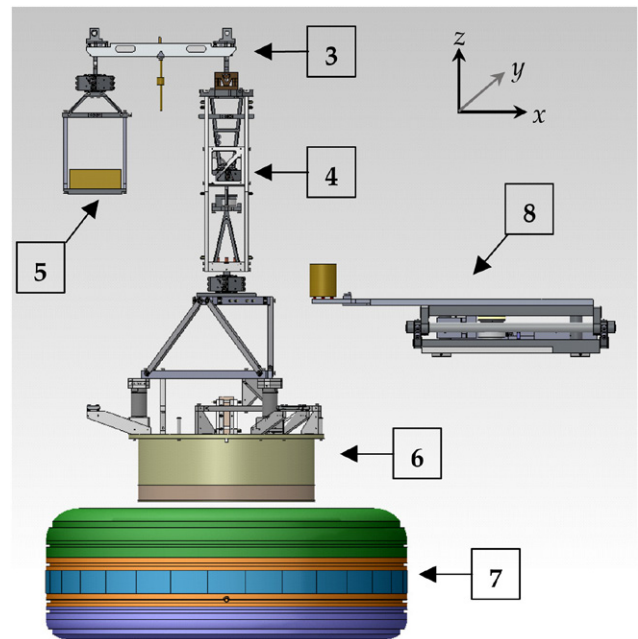

Figure 2. Schematic of the force comparator (3), its suspensions (4, 5) including the coil (6), the magnetic circuit (7) and the mass exchanger (8). Coordinate system: z axis point upwards, whereas x axis is parallel to the beam.

3.1. Translation stage

The translation stage is represented in the upper section 1 in figure 1. Its moving part is linked to the support structure of the watt balance by means of six sets of flexure hinges that constrain its movement to take place along only one direction [19, 20]. The adjustment of the parallelism of the hinge axes allows one to reduce the directional deviations of movement and

unwanted rotations around the horizontal axis. The total stroke of the guiding stage is 72 mm. Measurements are made in the central 40 mm portion of this. In this region, we have established prior to measurement of *h* that lateral deviations of the guiding stage from the vertical trajectory are below 0.5 µm and unwanted rotations in the horizontal plane are below 5 µrad.

Once unidirectional motion has been obtained, the direction of the stroke is adjusted to lie along a vertical reference axis defined by a precision tiltmeter. The procedure, based on the determination of the position of the centre of a metallic sphere fixed to the guiding stage by means of capacitive sensors, enables one to adjust the verticality to better than 10 µrad.

The main elements of the force comparator (balance beam and its suspensions) are fixed to the lower plate of the guiding stage. It is shown in the lower section 2 in figure 1.

3.2. Force comparator

The force comparator (3) is based on a 200 g homemade aluminium alloy beam [21–23], with two symmetrical 100 mm length arms. The three pivots are constituted by 20 µm thick stainless steel flexure strips clamped at both ends.

The end flexure strips support on one side a simple suspension for the tare mass (5) and on the other side two suspensions (4) on the same vertical axis: one is to receive a 500 g mass standard and the other is to fix the coil. These suspensions are articulated in their middle by the mean of clamped flexure strips gimbals. The suspensions of the mass and the coil are linked together with an electro-machined double monolithic gimbal [24] specially designed to reduce the effect of mutual static and dynamic coupling and to merge the points of application of the gravitational and Laplace forces.

The force comparator have a total mass of 6.2 kg (0.5 kg of which is due to the standard mass) hanging on the central flexure strip of the beam.

3.3. Coil and magnetic circuit assembly

The coil (6), made up of eight superimposed layers of a total of 684 windings of mean diameter 268 mm, secured with epoxy resin, is wound on a Delrin polymer support. The copper wire, insulated by a 15 µm polyesterimide layer has a diameter of 250 µm. Its resistance of 200 Ω leads to dissipated power of only 5 mW for a 5 mA nominal current.

The magnetic circuit (7) is of a loud-speaker type. The central ring made up of sixty samarium cobalt Sm_2Co_{17} permanent magnets is inserted between two XC48 steel plates. This assembly is surrounded by two yokes composed of two soft magnetic materials: pure iron and iron-cobalt alloy. The geometry of the yokes defines a 9 mm thick and 90 mm long air gap where the magnetic induction field, reaching 0.94 T, presents a minimum value. This minimum defines the position at which the coil is placed during the static phase in order to minimize the influence of its positioning error.

The geometry of the magnetic circuit, the choice of the different materials, the influence of magnetostriction, the machining and the mounting of the circuit have already been described extensively [25].

During mounting, the orientation of the radial magnetic field was made horizontal in a two-step procedure [26]. The first one, performed outside the watt balance structure, consists in tilting the magnet to make the field horizontal. To this end the Faraday effect probe is used to measure the orientation of the magnetic field with respect to the upper surface of the magnetic circuit. The second step, after the transfer of the magnetic circuit in the enclosure, consists in reproducing the upper surface orientation by means of a precision tiltmeter and a capacitive probe. At final, the mean magnetic plane is horizontal with an uncertainty of 10 µrad. The horizontality has been checked before this determination of the Planck constant.

3.4. Mass exchanger

The last element we describe is the mass exchanger (8). It has been developed to bring the standard mass onto the mass pan during the static phase (horizontal translation of 170 mm) and to lift it (maximum vertical translation of 6 mm) if necessary. In this way, the mass is removed during the dynamic phase.

The horizontal movement is guided by means of a commercial slide while the straightness of the vertical movement results from the use of a pantograph. For both movements, linear piezo-electric motors are used in a closed loop configuration with high-resolution linear encoders as position sensors. The horizontality of the mass exchanger is adjusted to allow the self centring of the mass on the pan. In addition to minimize mass pan oscillations the vertical velocity is kept at 10 µm s^{-1}.

4. Measurement considerations

4.1. Static phase measurement

After the two arms of the beam have been balanced in terms of mass, a tare mass equal to half the standard mass is added to the counterweight of the tare side. During the static phase, when the 500 g mass standard is placed on the pan (step 'on'), there is an excess weight of 250 g on the double suspension side and a stabilized current produces an electromagnetic force to compensate it. When the mass is removed (step 'off'), the same excess weight is on the tare suspension side and the current going through the coil is reversed to produce a force in the opposite direction: in both steps, the beam is balanced. This procedure was adopted to cancel the effect of the relative difference length of the two arms (by using only one arm to compare forces) and also to reduce the parasitic electromotive force in the electrical circuit (by reversing the current in the coil). By combining these two steps, one can evaluate the ratio *mg/I* which corresponds to the product $(B \cdot l)_{stat}$ of the static phase.

The different parameters to be evaluated are the mass *m*, the acceleration of gravity *g* and the current *I*:

- All measurements have been performed with a 500 g mass standard *m* made from XSH Alacrite which has been calibrated by the department of mass and derived quantities at the LNE.

- The absolute gravity value *g* is obtained with an absolute cold atom gravimeter (CAG) [27] operating near the watt balance since 2009. It has been regularly compared with other absolute gravimeters, especially during the three last key comparisons [28, 29]. A 3D gravity map combined with a model of the gravitational field in the laboratories [30] allow one to transfer the absolute value of gravity at the center of mass of the watt balance mass artifact under test. Finally, the self-attraction effect of the watt balance itself is also taken into account using the methods developed for the calculation of the self-attraction effect of the CAG [31].

- The current *I* is measured by the voltage drop (0.915 V) produced at the terminals of a 200 Ω standard resistor composed of two 100 Ω TGAM resistors in series and calibrated by comparison with a quantum Hall resistance. The current which traverses the coil is adjusted permanently by a real-time controller that includes a proportional-derivate algorithm driving a programmable current source in such a way that the balance beam is maintained at its equilibrium position. This position is checked with a detector based on the interception of a laser beam by a screen fixed at the extremity of the balance beam arm whose position must be determined. The power transmitted, measured by a photodiode, is proportional to the integral of the transmitted part of the Gaussian beam, i.e. proportional to a Gauss error function. The dynamic range and the sensitivity of the detector may be tuned by adjusting the diameter of the beam. This detector enables one to follow the displacement of the beam on a 50 μm range with a resolution better than 10 nm. The current source can deliver currents comprised between −5 mA and +5 mA. In order to provide sufficient resolution, two 16 bits DACs (coarse and fine) are used and their output voltages added before conversion to current. The stability of the current source operated in closed loop and controlled by comparison with a Josephson effect reference by means of a standard resistor reaches a 1×10^{-9} relative Allan deviation in 30 s.

The voltage drop at the terminals of the resistor is measured with three Agilent 3458 voltmeters used successively in cycles with an electronic system of synchronisation specially developed to eliminate 'dead time' between readings without cancelling the autozero function of the voltmeters. These voltmeters are calibrated daily by comparison against a Zener diode voltage standard itself directly calibrated against a Josephson standard.

4.2. Dynamic phase measurement

During the dynamic phase, the force comparator is moved vertically (see performance of the translation stage in 3.1) on a 14 mm range travel. At the beginning and the end of the movement, the acceleration is first increased linearly with time and then decreased to zero. Outside the period of acceleration, the velocity is maintained at $v_z = 2 \, \mathrm{mm \, s^{-1}}$. This movement induces a voltage *U* around 1 V at the terminals of the coil

(which is entirely immersed in the air gap of the magnetic circuit).

The quantities *U* and v_z are measured: the ratio U/v_z corresponds to the product $(B \cdot l)_{\mathrm{dyn}}$ of the dynamic phase.

The voltage *U* is measured by means of three Agilent 3458 A voltmeters in the same way as for the static phase and v_z is measured by three heterodyne Michelson interferometers [32] lighted by a frequency doubled stabilized Nd:YAG laser. The moving arms of the interferometers are comprised by three corner-cube reflectors located at the periphery of the coil support (placed at 120° from each other). The interferometers determine not only the vertical velocity v_z but also the angular velocities around the horizontal axis.

Three other position sensors are used to measure positions and velocities in the horizontal plane as well as the angular position and velocity around the vertical axis. They are based on vertical propagating gaussian beams intercepted by screens located at the periphery of the coil support.

Attention has been paid to measure simultaneously *U* and v_z so as to achieve maximal noise rejection: indeed the rejection ratio obtained is close to 100. To do this, the triggering signals issued from the voltmeters are also shaped in a sequence used to trigger the velocity measurements during the dynamic phase. In this case, there is a maximum delay of 1 μs between voltage and velocity measurements due to time resolution of the FPGA used to determine the interferometric phase which is more than five orders of magnitude smaller than the duration of one measurement of velocity and voltage (200 ms).

4.3. Environment condition measurements

All measurements were performed in air after the enclosure of the watt balance has been sealed. Temperature, pressure, humidity and carbon dioxide content were measured continuously during the experiment. The air density and refractive index were calculated using [33, 34] in order to apply corrections to the results. An example of the determination of these relative corrections is given in figure 3 which corresponds to a one week period.

5. Results

Software has been developed with the ability to construct a full measurement sequence from a set of elementary steps corresponding to the configuration of each device. Environmental conditions, calibration and measurement data are then stored and exploited *a posteriori*.

5.1. Dynamic phase: determination of the product $(B \cdot l)_{\mathrm{dyn}}$

A typical sequence of the dynamic phase consists of 100 pairs of up and down trajectories. Every trajectory is described by 40 data points and takes 8 s. A spatial profile of the product $(B \cdot l)_{\mathrm{dyn}}$ is then extracted and averaged over the set of the 200 steps. An example is shown in figure 4. As expected, the resulting shape goes through a minimum at mid-height of the
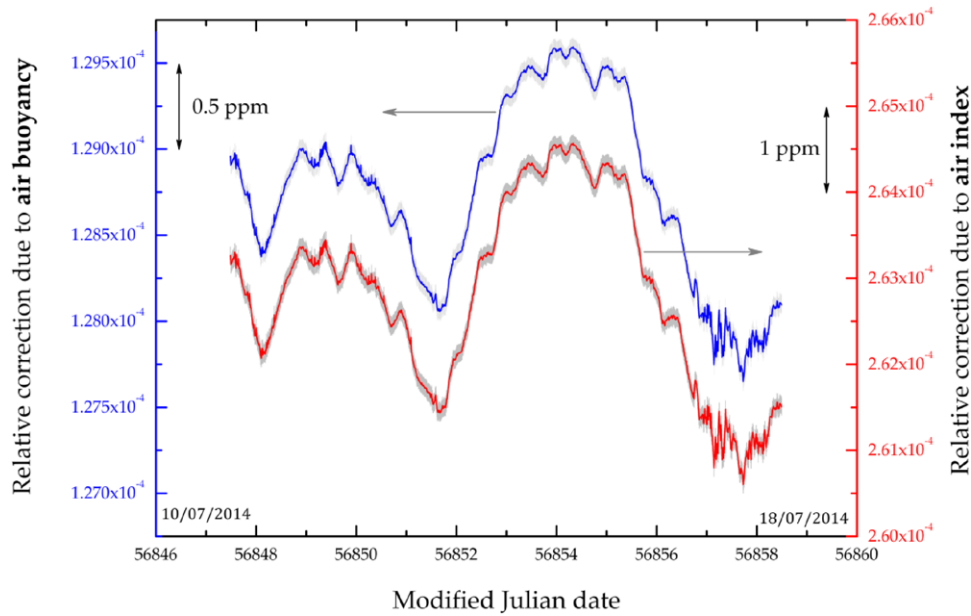
Figure 3. Evolution of the relative corrections in terms of *h* determinations due to air index and air buoyancy during one week. The gray areas stand for the uncertainty associated.
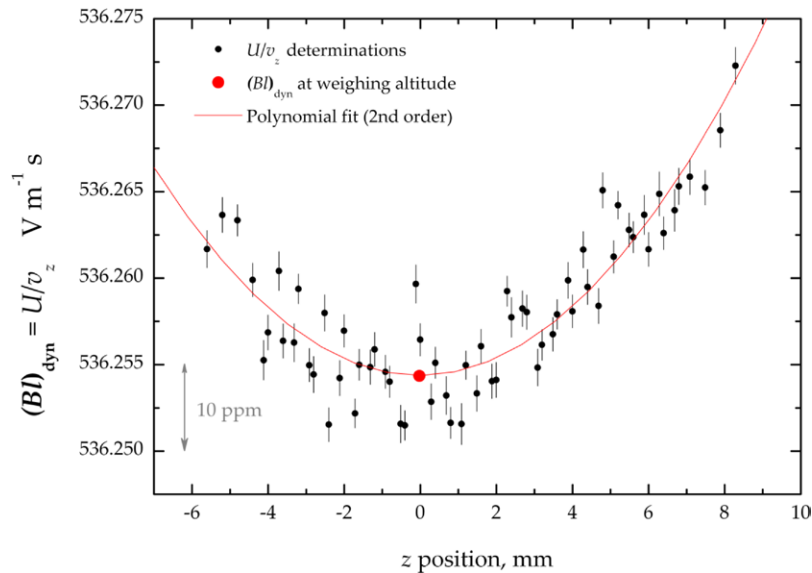

Figure 4. Product $(B \cdot l)_{\mathrm{dyn}} = U/v_z$ obtained during one sequence of 100 up and down trajectories. The red curve is the 2nd order polynomial fit, together with the estimation of $(B \cdot l)_{\mathrm{dyn}}$ at weighing altitude. Uncertainties shown are an evaluation of type A.

magnet gap. By fitting a second order polynomial curve to the data (red curve) we determine the value $(B \cdot l)_{\mathrm{dyn}}$ of the height at which the weighing phase takes place.

5.2. Static phase: determination of the product $(B \cdot l)_{\mathrm{stat}}$

A typical sequence of the static phase consists of ten pairs of 'mass on' and 'mass off' steps.

For both kind of step, the coil current is continuously adjusted by a programmable current source to oppose any change in the forces acting on the beam. However, from one step to another step, the current changes in response to force changes are not fast enough to maintain the beam in a horizontal position. It takes 100 s for the beam position to reach the steady state. Once the beam has reached its equilibrium position, 250 voltage readings taken with a 200 ms integration time are averaged to give the current I^{on} value in the configuration 'mass on'. After this measurement, the mass is raised by 1 mm ('mass off'), the vertical translation being made at a velocity of $10 \, \mu\mathrm{m \, s^{-1}}$. In the same way, the value of the current I^{off} in the configuration 'mass off' is determined. In practice, the process 'mass on' / 'mass off' is repeated 10 times and the final value of the current for the sequence is given by the relation:

$$I = \frac{1}{9} \sum_{i=1}^{9} \left[\left(\frac{I_{i+1}^{\mathrm{on}} + I_i^{\mathrm{on}}}{2} \right) - I_i^{\mathrm{off}} \right] \qquad (6)$$
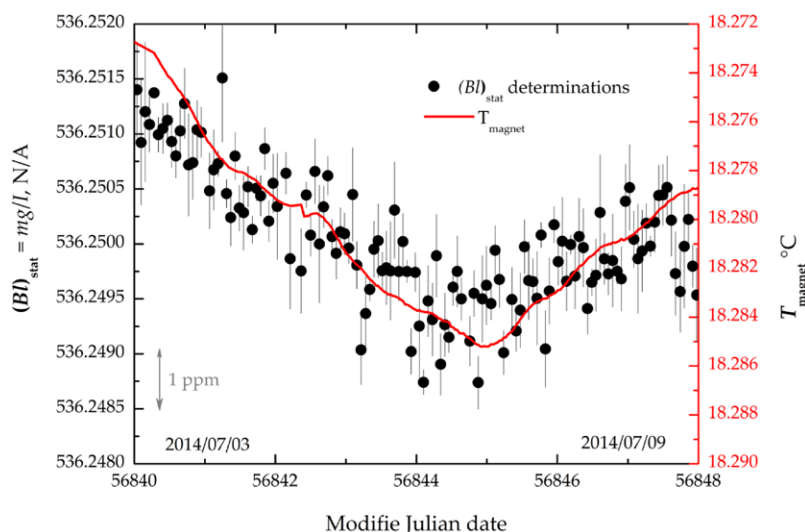
Figure 5. Variation of the product $(B \cdot l)_{stat} = mg/I$ during the static phase over the course of one week. The red line corresponds to the evolution of the magnet temperature. Uncertainties shown are a type A evaluation.
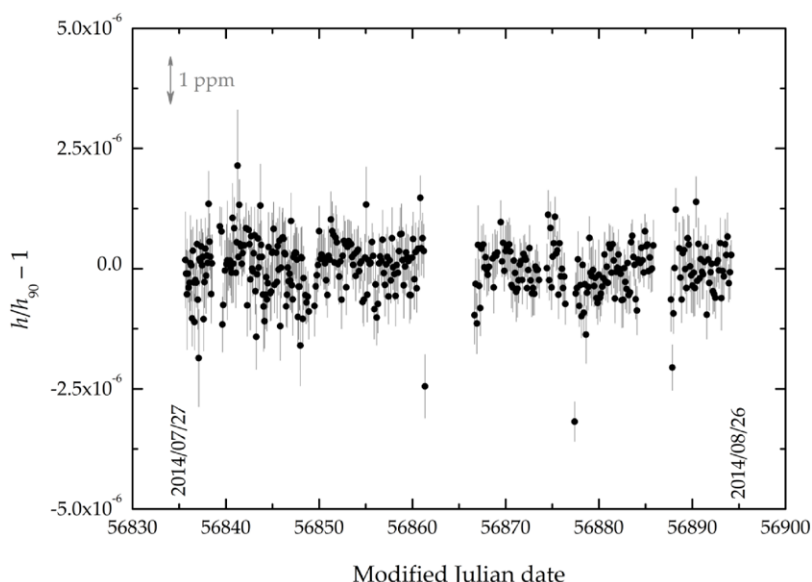

Figure 6. Set of data used for the determination of the Planck constant. Each black full dot represents an independent determination of *h*. Uncertainties shown are a type A evaluation of individual *h* determinations.

The knowledge of the mass, the acceleration of gravity and the measurements of the current *I* flowing through the coil allow one to evaluate the product $(B \cdot l)_{stat} = \frac{mg}{I}$. Figure 5 shows how this product varies over the course of one week (black circles). As expected, because of the temperature coefficient of the samarium-cobalt magnet (Sm_2Co_{17}), approximately $-3 \times 10^{-4} \, K^{-1}$, the observed change is correlated with the change in temperature (red curve). Note that two successive static determinations are separated by a dynamic phase.

5.3. Determination of the Planck constant from electrical and mechanical factors

Two successive values of *h* are determined in two different ways by considering:

- a first dynamic phase with one hundred pairs of up and down trajectories, a static phase with ten pairs of 'mass on' and 'mass off' and a second dynamic phase with one hundred pairs of up and down trajectories;
- or a first static phase with ten pairs of 'mass on' and 'mass off', a dynamic phase and a second static phase with ten pairs of 'mass on' and 'mass off'.

Each determination is then composed of three steps which are not processed at the same time and to take into account the drift due to the temperature changes of the magnet, a linear interpolation is performed between two successive values of $(B \cdot l)_{dyn}$ which is combined with one value of $(B \cdot l)_{stat}$. The same applies for two successive values of $(B \cdot l)_{stat}$ combined with one value of $(B \cdot l)_{dyn}$. More than 420 values were calculated during the summer of 2014. Results are presented in figure 6 where each point (black
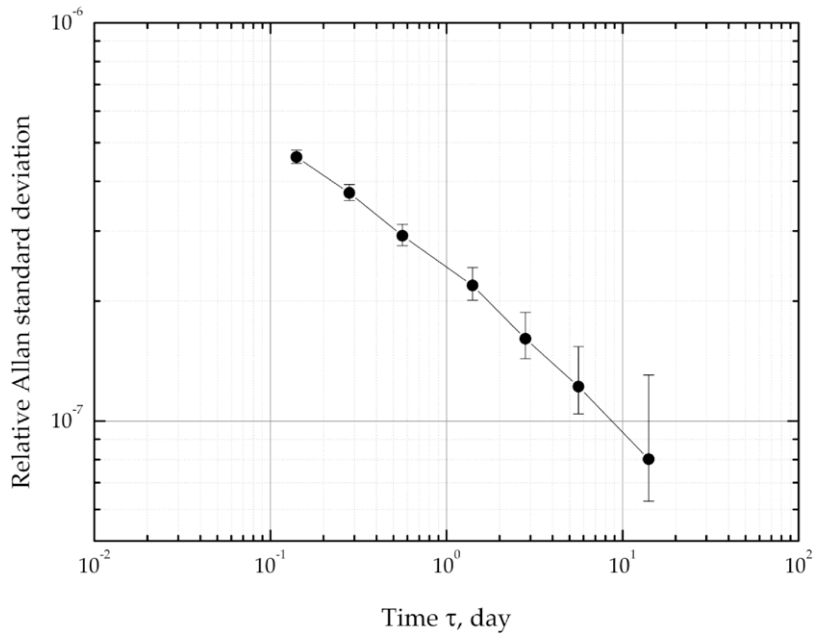
Figure 7. Relative Allan deviation of *h* measurements versus time.

full dot) corresponds to an independent value of *h* with its standard deviation. The gaps observed between some data were used for checks.

The value of *h* extracted from these data is $6.626\,068\,8(20) \times 10^{-34}$ Js which is lower than the h_{90} value by -0.05×10^{-7} in relative terms. The relative type A standard uncertainty is considered equal to the relative Allan deviation and estimated to be 8×10^{-8} (figure 7).

6. Uncertainty contributions and discussion

The main uncertainty contributions are summarized in table 1.

For this first determination of *h* with the LNE watt balance, the relative combined standard uncertainty amounts to 3.1×10^{-7}. Only the major uncertainty contributions are discussed in the following.

The *h* value reported here does not take into account the correction on the calibration of the French primary mass standard (copy n°35) due to the deviation of 35 µg on the unit of mass maintained at the BIPM discovered from the extraordinary calibrations carried out in 2014. The correction on the LNE *h* value amounts to -3.7 parts in 10^9 with an uncertainty of 3 parts in 10^9, so negligible in respect with the total uncertainty [35].

6.1. Major contributions for the $(B \cdot l)_{stat}$ determination

The product $(B \cdot l)_{stat}$ is given by the ratio of the weight of the standard mass to the total current injected in the coil. The measurements is made in two steps, with either a direct or a reversed current flowing through the coil for the configurations 'mass on' and 'mass off'. In both cases, a voltage drop is measured at the terminals of a 200 Ω resistor.

The uncertainties associated with the $(B \cdot l)_{stat}$ determination without taking into account the effects of the parasitic

Table 1. Main uncertainty contributions.

Uncertainty budget for *h* measurements	$k = 1$
Type A	8×10^{-8}
Type B	
Voltage measurements U' and U	2.4×10^{-7}
Resistance R	6×10^{-9}
500 g Alacrite mass (including traceability to the national prototype of the kilogram, buoyancy, magnetic susceptibility and alacrite density contributions)	7.4×10^{-8}
Absolute gravity value g	5×10^{-9}
Velocity v (including air refractive index and verticality of the laser beams)	1.2×10^{-7}
Parasitic watt ratio term (see equation (7))	9.1×10^{-8}
Force comparator contribution	3.3×10^{-8}
Other contributions (switch effect[a], polynomial fitting[b], trigger delay, hysteresis of the flexure strips)	5×10^{-8}
Combined relative uncertainty	3.1×10^{-7}

[a] The switch effect term concerns the performance of the commercial Data Proof low thermal scanner used for automating measurements of the static and dynamic phases.
[b] The 3rd and 4th order polynomial fits have been also tested and the differences obtained compared to the second order are lower than 5×10^{-8}. Moreover, the histogram of the residual of the second order adjustment is gaussian contrary to the 3rd and 4th. Considering that the relative standard uncertainty associated with *h* measurements is 3.1×10^{-7}, these differences have been considered, for the moment, as negligible contributions.

forces (see 5.3 and 5.4) are due to voltage measurements, resistance measurements and mass contributions.

6.1.1. Voltage measurements. The voltmeters are used in the 1 V range and are calibrated by a Zener voltage standard. The main relative standard uncertainty component is due to the gain stability of the voltmeters estimated to be 1.2×10^{-7} V. Other contributions are smaller as shown in table 2.

6.1.2. Resistance measurements. The 200 Ω resistor placed in a thermo-controlled enclosure (within ± 10 mK) is calibrated

Table 2. Source of voltage measurement uncertainties.

Uncertainty budget for voltage measurements in volt	$k = 1$
- Voltmeter calibration against Zener voltage reference (stability)	1.2×10^{-7}
- Zener source calibration against Josephson standard	1.1×10^{-8}
Relative combined uncertainty	1.2×10^{-7}

Table 3. Source of uncertainties in the resistance measurements.

Uncertainty budget for resistance measurements	$k = 1$
- Resistance calibration against QHRS	4×10^{-9}
- Stability of the resistors	5×10^{-9}
- Temperature effect	$<1 \times 10^{-9}$
- Power coefficient ($0.8 \times 10^{-9}\,\mathrm{mW^{-1}}$)	$<1 \times 10^{-9}$
- Time drift ($0.2 \times 10^{-9}\,\mathrm{d^{-1}}$)	$< 1 \times 10^{-9}$
Relative combined uncertainty	6×10^{-9}

against a quantum Hall resistance standard (QHRS). The total relative standard uncertainty associated with the resistance determination is 6×10^{-9}. The uncertainty budget is given in table 3. The main uncertainty component, which arises from the instability of the resistor due to its being moved to and from the QHRS room located 20 m away from the watt balance room does not exceed 5 parts in 10^9.

6.1.3. Mass contributions.

The mass used for the experiment is made from a cobalt-based superalloy, commercially known as XSH Alacrite, supplied by the French company Aubert-et-Duval. This mass artifact which density is 9 149 kg m^{-3} was polished and adjusted at the CNAM in the 1980s. Its mass stability studied over many years is equivalent to that of the best standard made from Pt-Ir alloy. The density and the mass have been measured by the LNE department of mass with respectively a standard uncertainty of 0.27 kg m^{-3} and 16 μg.

To take into account the buoyancy contribution and apply the associated correction to the mass, the air density has been calculated with an uncertainty of 5.4×10^{-4} kg m^{-3} by measuring temperature, pressure, relative humidity and mole fraction of carbon dioxide.

In addition, due to the presence of a residual magnetic field of 1.5 mT at the standard mass location, the magnetic susceptibility $+1.34 \times 10^{-3}$ of the mass introduces a significant undesired magnetic force of 3.7×10^{-7} N. The resulting error on the mass determination is 37 μg. This error has been corrected and its associated relative uncertainty is estimated to be 30%, i.e. 11 μg.

Finally, the relative standard uncertainty of the 500 g Alacrite mass (including traceability to the national prototype of the kilogram, buoyancy, magnetic susceptibility and alacrite density contributions) is 7.4×10^{-8}.

6.2. Major contributions for the $(B \cdot l)_{\mathrm{dyn}}$ determination

The product $(B \cdot l)_{\mathrm{dyn}}$ is given by the ratio of the induced voltage at the terminals of the coil to the velocity of the coil. Measurements are made when the coil is translated vertically (up and down) through the air gap of the magnetic circuit.

The uncertainty associated with the determination of $(B \cdot l)_{\mathrm{dyn}}$ is composed of both voltage and velocity measurements.

The first contribution has already been discussed above. Taken into account the correlation between the two successive voltage measurements (dynamic then static phases), the contribution of the two voltage measurements is added: the total voltage contribution is then equal to 2.4×10^{-7} in relative value.

The second contribution is due essentially to the air refractive index (1×10^{-7}) and to the verticality of the three laser beam directions. The verticality was determined with a standard uncertainty of 350 μrad which translates into a relative standard uncertainty for the power of 0.6×10^{-7}.

In total, the relative standard uncertainty associated with the velocity is 1.2×10^{-7}.

6.3. Watt ratio error term

Equation (3) was established for an ideal case free of unwanted parasitic forces and torques and unwanted horizontal and angular velocities. If one takes these parameters into account, the equation becomes:

$$\frac{U \cdot I}{F_z \cdot v_z} = 1 + \frac{F_x \cdot v_x}{F_z \cdot v_z} + \frac{F_y \cdot v_y}{F_z \cdot v_z} + \frac{\tau_x \cdot \omega_x}{F_z \cdot v_z} + \frac{\tau_y \cdot \omega_y}{F_z \cdot v_z} + \frac{\tau_z \cdot \omega_z}{F_z \cdot v_z} \quad (7)$$

where F_i is the force along the ith axis and v_i is the velocity along that axis. τ_i is the torque about the ith axis and ω_i is the angular velocity about that axis. The vertical velocity v_z is 2 mm s^{-1}, whereas the vertical force F_z (nominally equal to the weight of the standard mass m) is 4.9 N.

The five latter terms in the equation above are referred to as the parasitic watt ratio error term.

Using the double pendulum mathematical model [36, 37], and the different experiments described in [38], we have estimated the parasitic forces and torques during this campaign of measurements. By using the three gaussian position detectors and the three heterodyne Michelson interferometers, the horizontal and angular velocities were estimated during measurements of h. The watt ratio error was found to lie within $\pm 1.6 \times 10^{-7}$ (table 4). If one assumes a rectangular distribution, the relative standard uncertainty associated is 9.1×10^{-8}.

From table 4, it worth noting that:

(a) The ratios v_x/v_z and v_y/v_z of the coil should be of the order of 1.2×10^{-5}, considering the performance of the translation stage (the lateral deviations from the 40 mm vertical trajectory are below 0.5 μm). The values measured are higher by more than two orders of magnitude. This could be due to the fact that the three laser beams which intercept the three screens fixed at the periphery of the coil support (placed at 120° from each other) are not vertical (at better than 1 mrad), however this is currently under investigation. We nevertheless use measured velocities as an overestimation of the parasitic velocities of the coil.

(b) The force ratios are below 50×10^{-6}.

Table 4. Estimation of the watt ratio error term from relative parasitic velocities, parasitic forces and torques.

| Relative parasitic forces and torques		Relative parasitic linear and angular velocities		Individual component of watt ratio error term	
F_x/F_z	$<20 \times 10^{-6}$	v_x/v_z	$<2000 \times 10^{-6}$	$F_x.v_x/F_z.v_z$	$<4.5 \times 10^{-8}$
F_y/F_z	$<50 \times 10^{-6}$	v_y/v_z	$<1500 \times 10^{-6}$	$F_y.v_y/F_z.v_z$	$<7.5 \times 10^{-8}$
M_x/F_z	$<10 \times 10^{-6}\,\mathrm{m}$	ω_x/v_z	$<1000 \times 10^{-6}\,\mathrm{rad\,m^{-1}}$	$M_x.\omega_x/F_z.v_z$	$<1 \times 10^{-8}$
M_y/F_z	$<20 \times 10^{-6}\,\mathrm{m}$	ω_y/v_z	$<1000 \times 10^{-6}\,\mathrm{rad\,m^{-1}}$	$M_y.\omega_y/F_z.v_z$	$<2 \times 10^{-8}$
M_z/F_z	$<10 \times 10^{-6}\,\mathrm{m}$	ω_z/v_z	$<1000 \times 10^{-6}\,\mathrm{rad\,m^{-1}}$	$M_z.\omega_z/F_z.v_z$	$<1 \times 10^{-8}$
				Watt ratio error	$<1.6 \times 10^{-7}$
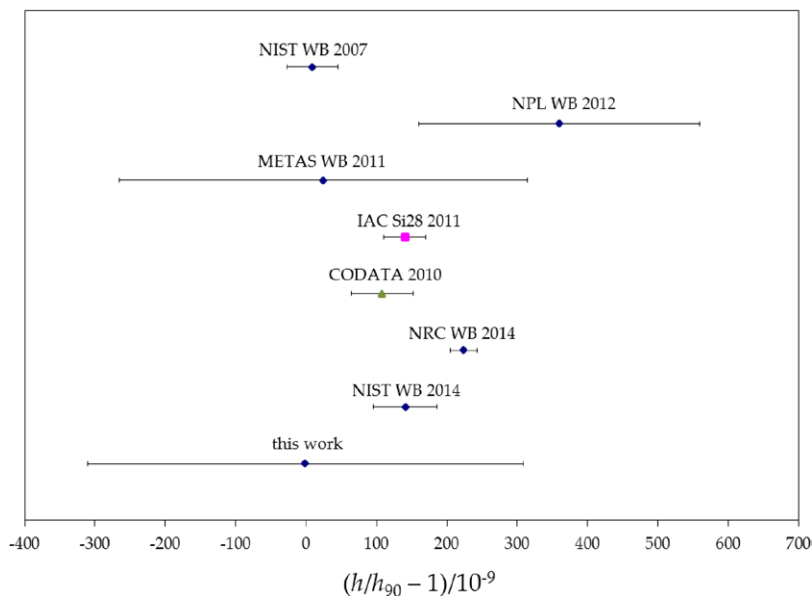
Figure 8. Summary of recent determinations of the Planck constant with watt balances. A silicon sphere determination is added as well as the last CODATA recommendation. Values are referred to the h_{90} value. (For watt balances results, see [9, 12, 41, 42, 45]; for IAC silicon sphere, see [43]; for CODATA, see [44].)

6.4. Force comparator contribution

Because the comparator is not used as a mass comparator, the horizontality of its pivots is of great importance. Indeed, for a non-horizontal position, parasitic forces introduce a systematic error in the weighing. To make this error negligible, either the comparator is aligned horizontally or the parasitic forces are nulled. At present, it is not possible to adjust the angular position of the pivot axis of the beam to better than 3 mrad relative to the horizontal. For this reason, we must take into account the contribution of the parasitic forces along the mass comparator (F_x estimated smaller than 90 μN, or 20 ppm in relative term) during the weighing. The contribution of these alignments to the relative standard uncertainty is then evaluated to 3.3×10^{-8}.

7. Conclusion

Measurements of the Planck constant h were performed in air during the summer of 2014. The value $6.626\,068\,8(20) \times 10^{-34}$ Js has been extracted from these data. It differs in relative terms by -0.05×10^{-7} from the h_{90} value (figure 8) and by -1.1×10^{-7} from that of the 2010 CODATA adjustment of h. The relative standard uncertainty associated with this measurement 3.1×10^{-7} is thus larger than these differences.

Currently, the major contributions to the published uncertainty arise from voltage measurements, velocity measurements and suspension alignments. These contributions are not yet a limitation of our experiment and it will certainly be possible to reduce them. To achieve this, several works are planned, and notably:

- Voltage measurements during static and dynamic phases will be made directly against a 1 V programmable Josephson voltage standard (PJVS) [39, 40], available in the laboratory.
- Some improvements will be implemented to adjust the verticality of the six gaussian laser beams (going through the position detectors and the corner cubes of the coil) using a mercury pool and a 1.1 m focal length telescope.
- Another 500 g mass artifact, made from Pt–Ir alloy provided by the English company Johnson–Matthey, and polished, adjusted and calibrated by the BIPM will be used for the next campaign of measurements, notably because its magnetic susceptibility is lower than that of Alacrite and its density is higher.

References

[1] Quinn T J 1991 The kilogram: the present state of our knowledge *IEEE Trans. Instrumen. Meas.* **40** 81–5

[2] Davis R 2003 The SI unit of mass *Metrologia* **40** 299

[3] Girard G 2005 The third periodic verification of national prototypes of the kilogram (1988–1992) *Metrologia* **31** 317

[4] Bordé C J 2004 Métrologie fondamentale : unités de base et constantes fondamentales C. *R. Phys.* **5** 813–20

[5] Mills I M, Mohr P J, Quinn T J, Taylor B N and Williams E R 2005 Redefinition of the kilogram: a decision whose time has come *Metrologia* **42** 71–80

[6] Mills I M, Mohr P J, Quinn T J, Taylor B N and Williams E R 2006 Redefinition of the kilogram, ampere, kelvin and mole: a proposed approach to implementing CIPM recommendation 1 (CI-2005) *Metrologia* **43** 227–46

[7] Stock M and Witt T J 2006 CPEM 2006 round table discussion 'Proposed changes to the SI' *Metrologia* **43** 583–7

[8] Becker M 2001 History and progress in the accurate determination of the Avogadro constant *Rep. Prog. Phys* **64** 1945–2008

[9] Robinson I A 2012 Towards the redefinition of the kilogram: a measurement of the Planck constant using the NPL Mark II watt balance *Metrologia* **49** 113–56

[10] Williams E R, Steiner R L, Newell D B, and Olsen P T 1998 Accurate measurement of the Planck constant *Phys. Rev. Lett.* **81** 2404–7

[11] Thomas M, Espel P, Bielsa F, Genevès G, Piquemal F, Juncar P and Pinot P 2014 Progress report of the LNE watt balance *Conf. on Precision Electromagnetic Measurements (2014)* pp 426–7

[12] Sanchez C A, Wood B M, Green R G, Liard J O and Inglis A D 2014 A determination of Planck's constant using the NRC watt balance *Metrologia* **51** S5–14

[13] Fang H, Kiss A, Robertsson L, Zeggagh A, Lan J, de Mirandes E, Solve S, Picard A and Stock M 2012 Status of the BIPM watt balance *Conf. on Precision Electromagnetic Measurements (2012)* pp 424–5

[14] Eichenberger A, Baumann H, Jeckelmann B, Tommasini D, Cosandier F, Clavel R, Beguin C and Reber D 2012 The METAS watt balance Mark II experiment *Conf. on Precision Electromagnetic Measurements (2012)* pp 426–7

[15] Suton C M 2009 An oscillatory dynamic mode for a watt balance *Metrologia* **46** 467

[16] Zhang Z, He Q, Li Z, Han B, Lu Y, Lan J, Li S and Fu Y 2012 The Joule balance in progress *Conf. on Precision Electromagnetic Measurements (2012)* pp 432–3

[17] Kibble B P 1976 *A Measurement of the Gyromagnetic Ratio of the Proton by the Strong Field Method, Atomic Masses and Fundamental Constants* 5th edn ed J H Sanders and A H Wapstra (New York: Plenum) pp 545–51

[18] Mohr P J and Taylor B N 2000 CODATA recommended values of the fundamental physical constants: 1998 *Rev. Mod. Phys.* **72** 351

[19] Villar F, David J and Genevès G 2011 75 mm stroke flexure stage for the LNE watt balance experiment *Precis. Eng.* **35** 693–703

[20] Villar F 2008 Conception, réalisation et caractérisation de systèmes mécaniques pour l'expérience française de 'balance du watt' *Doctoral Thesis* Conservatoire National des Arts et Métiers—CNAM (http://tel.archives-ouvertes.fr/tel-00369283)

[21] Pinot P, Genevès G, Juncar P, Lecollinet M, Macé S and Villar F 2005 Expérience française de la balance du watt: conception et réalisation du comparateur de forces *Conf. Proc. of Congrès Int. de Métrologie (2005)* (available on CD edited by Collège Français de Métrologie)

[22] Pinot P, Genevès G, Haddad D, David J, Juncar P, Lecollinet M, Macé S and Villar F 2007 Theoretical analysis for the design of the French watt balance experiment force comparator *Rev. Sci. Instrum.* **78** 095108

[23] Pinot P 2010 Étude de lames flexibles en cuivre-béryllium pour l'expérience française de balance du watt *Revue Française de Métrologie* **2010–1** 21

[24] Pinot P, Mace S, Genevès G, Gournay P, Haddad D, Lecollinet M, Villar F and Himbert M E 2008 Dynamic behaviour of a monolithic suspension device for the French watt balance experiment *Eur. Phys. J. Appl. Phys.* **44** 193–204

[25] Gournay P, Genevès G, Alves F, Besbes M, Villar F and David J 2005 Magnetic circuit design for the BNM Watt balance experiment *IEEE Trans. Instrum. Meas.* **54** 742–5

[26] Ouedraogo K, Topsu S, Gayhmouni J, Chassagne L, Alayli Y, Juncar P, Gournay P, Bielsa F and Genevès G 2012 Accurate ellipsometric magnetic-field sensor used to align the watt balance magnetic circuit of the French National Metrology Institute *Sensors Actuators* A*: Phys.* **175** 9–14

[27] Louchet-Chauvet A, Farah T, Bodart Q, Clairon A, Landragin A, Merlet S and Pereira Dos Santos F 2011 Influence of transverse motion within an atomic gravimeter *New J. Phys.* **13** 065025

[28] Jiang Z *et al* 2012 The 8th international comparison of absolute gravimeters: the first key comparison (CCM.G-K1) in the field of absolute gravimetry *Metrologia* **49** 666–84

[29] Francis O *et al* 2013 The European comparison of absolute gravimeters 2011 (ECAG-2011) in Walferdange Luxembourg: results and recommandations *Metrologia* **50** 257–68

[30] Merlet S, Kopaev A, Diament M, Genevès G, Landragin A and Pereira Dos Santos F 2008 Micro-gravity investigations for the LNE watt balance project *Metrologia* **45** 265

[31] D'Agostino G, Merlet S, Landragin A and Pereira Dos Santos F 2011 Perturbations of the local gravity field due to mass distribution on precise measuring instruments: a numerical method applied to a cold atom gravimeter *Metrologia* **48** 299–305

[32] Haddad D, Juncar P, Geneves G and Wakim M 2009 Gaussian beams and spatial modulation in nanopositioning *IEEE Trans. Instrum. Meas.* **58** 1003–9

[33] Ciddor P E 1996 Refractive index of air: new equations for the visible and near infrared *Appl. Opt.* **35** 1566–73

[34] Picard A, Davis R S, Gläser M and Fujii K 2008 Revised formula for the density of moist air (CIPM-2007) *Metrologia* **45** 149–55

[35] Stock M 2014 BIPM, private communication

[36] Villar F, Genevès G and David J 2010 Determination and minimization of parasitic forces and moments in the static step of the LNE watt balance experiment *Conf. on Precision Electromagnetic Measurements (2010)* pp 34–5

[37] Genevès G 2011 Une méthode de détermination des effets de désalignement dans les expériences de balance du watt *Congrès International de Métrologie* (Paris: Collège français de métrologie)

[38] Thomas M, Espel P, Briand Y, Genevès G, Bielsa F, Pinot P, Juncar P and Piquemal F 2014 Minimization of the coil movement of the LNE watt balance during weighing mode and estimation of parasitic forces and torques involved *Metrologia* **51** S54–64

[39] Maletras F-X, Gournay P, Robinson I A and Genevès G 2007 A bias source for dynamic voltage measurements with a programmable Josephson junction array *IEEE Trans. Instrum. Meas.* **56** 495–9

[40] Genevès G, Gournay P, Hauck C, Djordjevic S and Behr R 2006 Characterisation of a SINIS programmable binary Josephson junction array as a reference for the French watt balance experiment *Conf. on Precision Electromagnetic Measurements Digest (2006)*

[41] Steiner R L, Williams E R, Liu R and Newell D B 2007 Uncertainty improvements of the NIST electronic kilogram *IEEE Tran. Instrum. Meas.* **56** 592–6

[42] Eichenberger A *et al* 2011 Determination of the Planck constant with the METAS watt balance *Metrologia* **48** 133

[43] Andreas B *et al* 2011 Determination of the Avogadro constant by counting the atoms in a ^{28}Si crystal *Phys. Rev. Lett.* **106** 030801

[44] Mohr P J, Taylor B N and Newell D B 2012 CODATA recommended values of the fundamental physical constants: 2010 *Rev. Mod. Phys.* **84** 1527–605

[45] Schlamminger S *et al* 2014 Determination of the Planck constant using a watt balance with a superconducting magnet system at the National Institute of Standards and Technology *Metrologia* **51** S15